NANO: Brief Reports and Reviews
Vol. 16, No. 10 (2021) 2150112 (8 pages)

DOI: 10.1142/S1793292021501125

Change of Bandgap Energy in Quantum System of Nanolayer on Silicon

Wei-Qi Huang*,†,§,‖, Zi-Lin Wang*, Cui-Fen Chen*, Ke Wang*, Hong-Yan Peng*,¶, Zhong-Mei Huang†, Xin Li†, An-Chen Wang† and Shi-Rong Liu‡

*Department of Physics, Hainan Normal University, Haikou 571158, China

†College of Materials and Metallurgy, Institute of Nanophotonic Physics, Guizhou University, Guiyang 550025, P. R. China

‡State Key Laboratory of Environment Geochemistry, Institute of Geochemistry, Chinese Academy of Sciences, Guiyang 550003, P. R. China

§wqhuang@gzu.edu.cn

¶mdjphy@163.com

Received 3 March 2021
Accepted 19 July 2021
Published 10 September 2021

In the quantum system of nanolayer (NL) on silicon, the bandgap energy obviously increases with the decrease of NL thickness, where the quantum confinement (QC) effect plays the main role as the thickness of Si NL changes along with (100), (110) and (111) directions, respectively. And the simulation result demonstrated that the direct bandgap can be obtained as the NL with (001) direction is thinner than 10 nm on Si surface. However, it is discovered in the simulated calculation that the QC effect disappears as the NL thickness arrives at the size of the monoatomic layer, in which its bandgap sharply decreases, where the abrupt change effect in bandgap energy occurs near-ideal 2D-layer. In the experiment, we fabricated the Si NL structure by using electron beam irradiation and laser deposition methods, in which a novel way was used to control the NL thickness by modulating irradiation time of the electron beam. The new effect should have a good application on a photonic-electronic chip of silicon.

Keywords: Silicon nanolayer; abrupt change effect; quantum confinement; bandgap; simulated calculation.

1. Introduction

The nanostructures have been investigated, mainly involving nanoparticles, nanowires and nanolayers in the past decade.[1–5] Especially, scientists have focused on the nanolayer (NL) structure due to its unique properties and applications, such as the

‖Corresponding author.

core/multishell nanostructures used to the high-efficiency light-emitting diodes,[6] the lasing from individual GaAs-AlGaAs on core-shell nanostructures,[7] optically pumped room-temperature GaAs lasers on the nanowire,[8] high-performance transistors on the nanowire[9,10] and the nanowire array solar cells with higher efficiency.[11] Recently, some interesting phenomena and new effects have been discovered in the quantum system of Si NL, where scientists have invested strong efforts to the growth of 2D silicon material,[12,13] which was named the silicene analogue of graphene. It was expected to have a great impact on the development of future electronic devices and energy storage.[14–16] In the last few years, the molecular dynamics simulation was used to study the nanosilicon, such as the formation of single- and double-layer silicons in slit pores, where their stability was further confirmed by first-principles calculation in the simulated calculation.[17,18]

Here, it is interesting that the quantum confinement (QC) effect plays the main role as the NL thickness is larger than 0.5 nm. The energy bandgap obviously increases with decreasing thickness of NL by the QC effect in the quantum system of NL on silicon. In the article, the QC effect has been exhibited as the thickness of Si NL changes along with (100), (110) and (111) directions, respectively, in simulating calculation. And the simulation result demonstrated that the direct bandgap can be obtained as the NL diameter is smaller than 10 nm in NL with (001) direction on Si surface. However, the bandgap energy of the NL changes in complicated ruler as the NL reaches to 2D Si material, where a new effect takes place on the energy change of the NL bandgap. The bandgap energy in a quantum system of Si NL abruptly decreases as the NL is near the 2D structure. It is discovered in the simulated calculation that the QC effect disappears as the NL thickness arrives at the size of the monoatomic layer, in which the abrupt change effect of bandgap energy occurs.

2. Experiments

Scientists usually used the self-assembly ways from silicon-rich silicon oxide matrices and plasma synthesis methods to fabricate various silicon nanostructures.[19–25] Here, the interesting method for fabricating silicon nanocrystal is grown under laser photons interaction.[26–28] We have taken the interesting and simplest method for fabricating silicon nanolayer (NL), in which Si NL crystal rapidly grows with irradiation of electron beam on amorphous silicon film prepared by using pulsed laser deposition (PLD). The novel method of electron affection could be used to replace the traditional annealing methods in the preparing process of silicon nanocrystals,[29] in which the thickness of nanolayers is easy to be controlled in growing with irradiation of the electron beam.

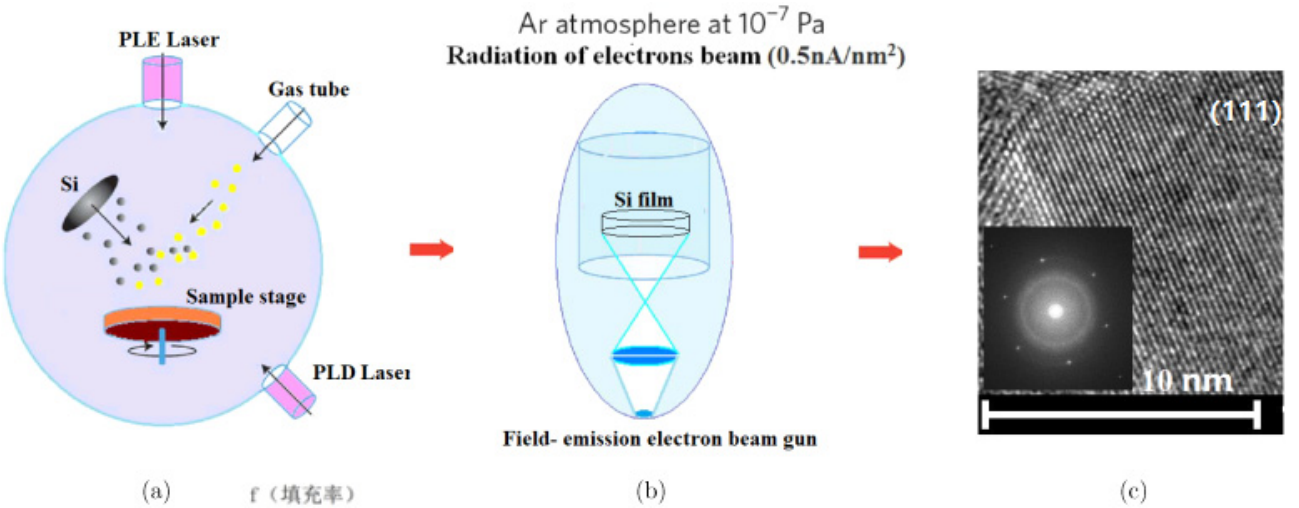

Fig. 1. Fabrication system of Si nanolayer with PLD and PLE devices. (a) Depiction of the PLD device with vacuum cavity and nanosecond pulsed laser. (b) Depiction of the coherent electron irradiation system with field-emission electron gun. (c) TEM image exhibiting a geometry top viewed on the NL structure of silicon, in which the inset shows its electron diffraction pattern.

We prepared the NL structures on silicon which involves two steps. At first, a nanosecond pulsed Nd:YAG laser and the third harmonic of pulsed Nd:YAG laser at 355 nm are used to deposit the amorphous nanolayers on a silicon chip in the PLD process. The silicon wafers of P-type substrate are taken on the sample stage in the fabrication system with PLD devices, in which the amorphous Si NL is prepared as depicted in Fig. 1(a). The pulsed laser etching (PLE) method is used to prepare micro-nanoarrays on Si substrate before the PLD process. Then the amorphous Si NL is exposed under electron beam with 0.5 nA/nm^2 for 30 min in Tecnai G2 F20 system, it can be observed that silicon nanocrystals rapidly grow with irradiation of electron beam and various thicknesses of nanolayers are gradually produced with different irradiation times, as depicted in Fig. 1(b).

The Transmission electron microscope (TEM) image exhibits a crystal geometry top viewed on the Si NL as shown in Fig. 1(c), in which the inset shows its electron diffraction pattern. Truly interesting, several structures of silicone with the quasi-2D film were obtained through controlling irradiation time and density of the coherent electron beam, which are, respectively, related to growing along with (100), (110) and (111) directions.

3. Investigation on Si Nanolayer in Simulation

The dynamic stability of the nanolayer was investigated by using first-principles calculations with consideration of three kinds of crystal structures observed in the experiment, in which the crystal lattice grows, respectively, along with (100), (110) and (111) directions. The electronic behavior on the Si NL was investigated by an *ab initio* nonrelativistic quantum mechanical analysis. Some physical models have been chosen in order to simulate various kinds of surface structures of nanosilicon. The models based on supercells have advantages that are simple and emphasize the quantum confinement effect and deformation of the surface structure. The density functional theory (DFT) was used to calculate the density of states (DOS) on silicon nanolayers, which is carried out with the local density approximation (LDA) and gradient-corrected exchange-correlation function (GGA) for the self-consistent total energy methods.

It is interesting in the total energy calculations using the DFT method that the transformation from the indirect bandgap to direct bandgap can be obtained as the nanolayer thickness is smaller than 10 nm, with the simulated model of NL structure along (001) direction, its direct bandgap and its DOS picture are shown in Figs. 2(a)–(c) after simulated calculation. It is originated from the Heisenberg principle related to $h\Delta K_x \sim h/\Delta x$, in

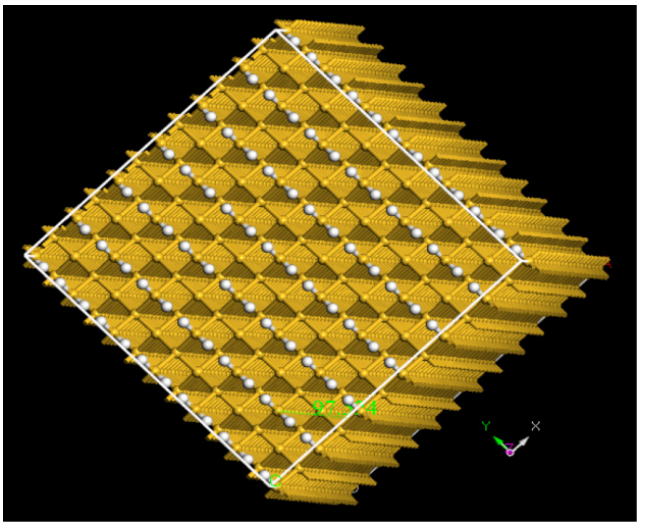

(a)

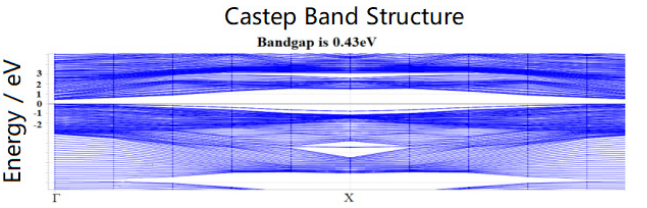

(b)

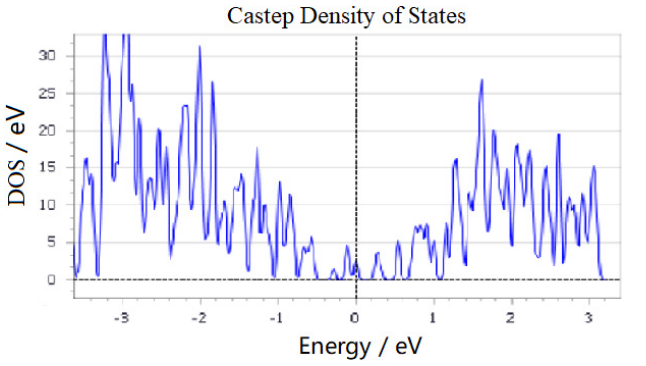

(c)

Fig. 2. (a) Simulated model of NL structure along with (001) direction. (b) Energy band construction of the NL structure along with (001) direction, in which the direct bandgap can be obtained. (c) DOS picture of the NL structure along with (001) direction.

which the wave vector will relax from the X region to Γ region as the Δx decreases to the nanoscale (relaxing relation: $\Delta x\downarrow \rightarrow \Delta K_x\uparrow$), where higher electronic speed is obtained in nanolayer.

In the experimental result, the nanolayer of silicon crystal growing along with (100) direction was prepared, as shown in Fig. 3(a), where the TEM image exhibits its structure. In the simulated calculation, the DMol3 mode is used to make an optimum atomic structure for obtaining the lowest combining energy, and the CASTEP mode is used to simulate for obtaining the energy band structure after the optimum process. In Fig. 3(b), the simulation model of the Si nanolayer has been built along with (100) direction according to the experimental result. After the optimization process in simulation, the quasi-2D structure of silicon crystal with the rectangular lattice occurs in the lowest energy of optimum structure, as shown in Fig. 3(c). The structural transformation from the ideal model of 2D structures to the optimal quasi-2D structures of Si crystal along with (100) direction should be noted in the simulation process, where the convex bonding angles take place on silicon film.

Figure 3(d) exhibitsthe change curve of bandgap energy with various thicknesses of Si NL along with (100) direction in the simulation result, where it is interesting that the quantum confinement (QC) effect plays the main role as the nanolayer thickness is lager, but the QC effect disappears as the nanolayer thickness is smaller than 0.4 nm near the monoatomic layer when its bandgap energy

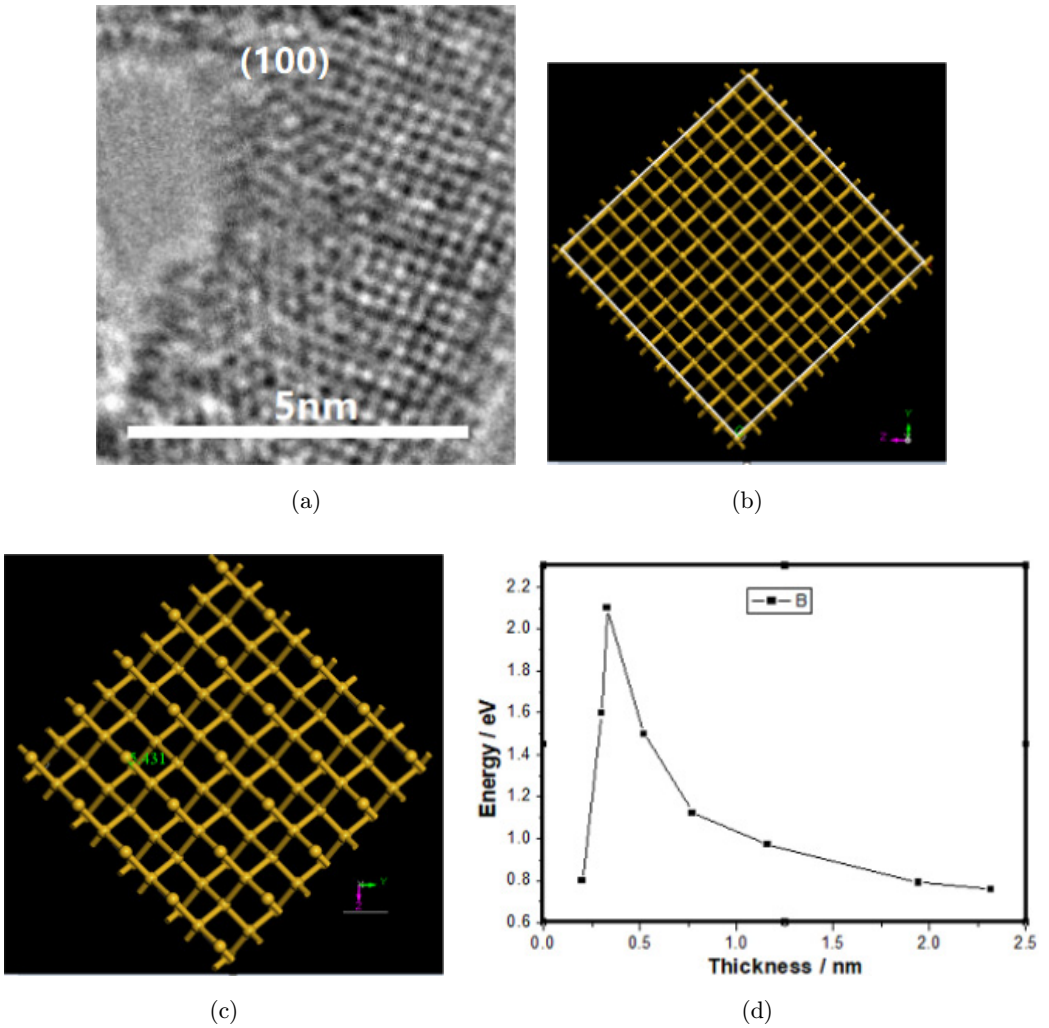

Fig. 3. (a) TEM image of Si NL crystal growing along with (100) direction. (b) Simulation model of the Si NL built along with (100) direction according to the experimental result. (c) Quasi-2D structure of the Si NL crystal with the rectangular lattice occurring in the lowest energy of optimum structure after the optimization process in simulation. (d) Change curve of bandgap energy with various thicknesses of Si NL along with (100) direction in the simulation result.

abruptly decreases. Truly interesting, the QC effect disappears as the nanolayer thickness reaches to the size of the monoatomic layer, where its bandgap sharply decreases. This abrupt change effect in bandgap energy may be originated from transforming between different dimensions at the symmetry broken point, in which the quasi-2D shape of NL is transformed to the two-dimensional quantum layer. Here, the abrupt change effect in bandgap energy was observed and studied at first.

The nanolayer structure of the Si crystal growing along with (110) direction was obtained, as shown in the TEM image of Fig. 4(a), from which we can build the simulation model of the Si nanolayer in this direction, as exhibited in Fig. 4(b). The idea model structure with the hexagonal lattice is transformed to the real quasi-2D structure with convex atomic bonds after the simulated optimum process, as shown in Fig. 4(c). In the same way, the abrupt change effect in bandgap energy takes place as the nanolayer thickness reaches the size of the monoatomic layer, where the QC effect disappears, as shown in Fig. 4(d). Here, it is interesting to make a compression between the quasi-2D silicene with the hexagonal lattice and the graphite. The simulation result demonstrates that the indirect bandgap can be transformed to the direct bandgap as the nanolayer thickness along with (110) direction is smaller than 3 nm.

In the same way, the TEM image in Fig. 5(a) shows the nanolayer structure of the Si crystal growing with (111) direction, according to whom the simulated model of the Si nanolayer in this direction can be built, as shown in Fig. 5(b). The real quasi-2D structure along with Si crystal (111) direction can be obtained after the simulated

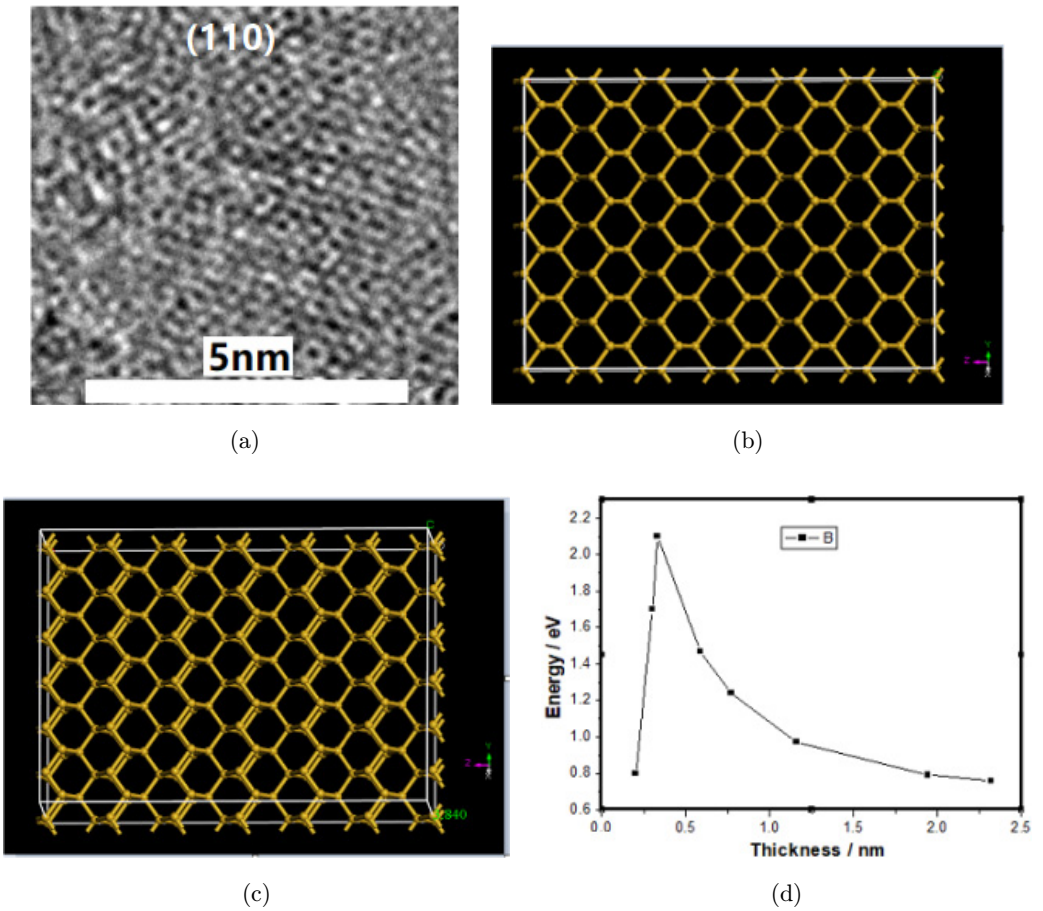

Fig. 4. (a) TEM image of Si NL crystal growing along with (110) direction. (b) Simulation model of the Si NL built along with (110) direction according to the experimental result. (c) Quasi-2D structure of the Si NL crystal with the hexagonal lattice occurring in the lowest energy of optimum structure after optimization process in simulation. (d) Change curve of bandgap energy with various thicknesses of Si NL along with (110) direction in the simulation result.

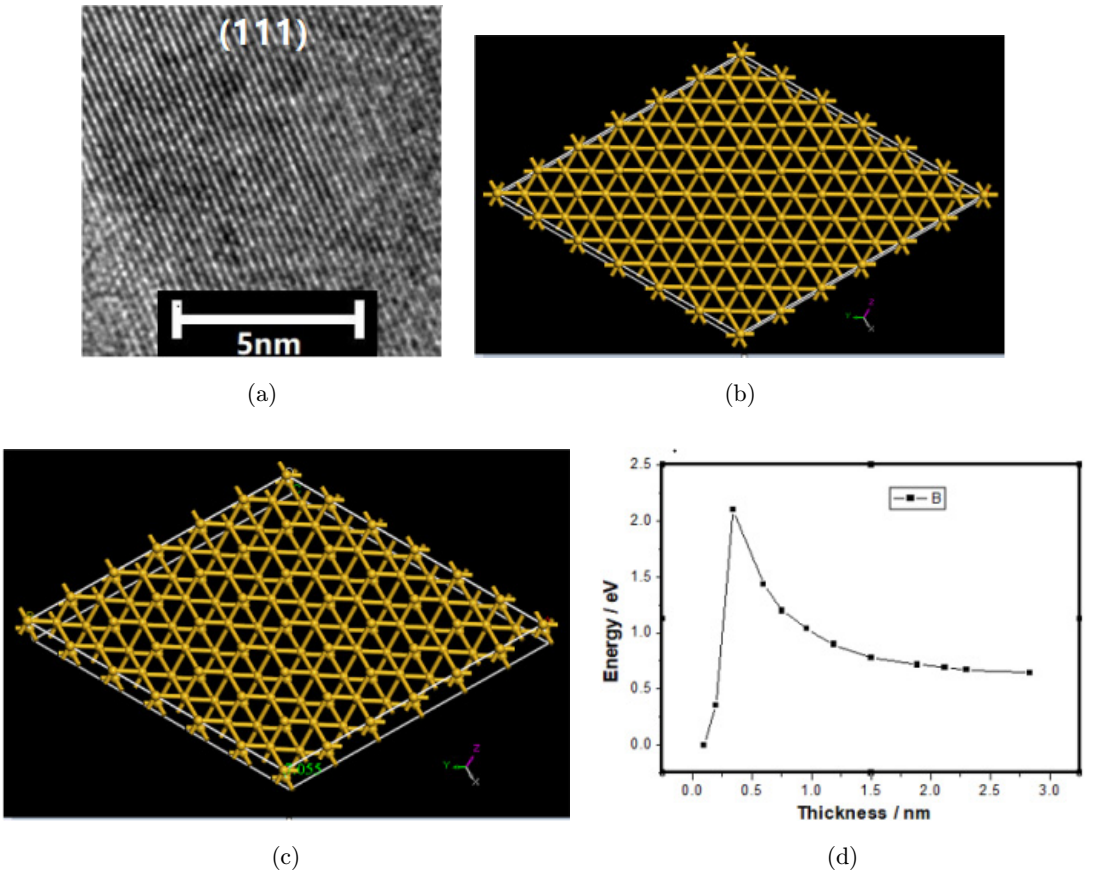

Fig. 5. (a) TEM image of Si NL crystal growing along with (111) direction. (b) Simulation model of the Si NL built along with (111) direction according to the experimental result. (c) Quasi-2D structure of the Si NL crystal along with (111) direction occurring in the lowest energy of optimum structure after optimization process in simulation. (d) Change curve of bandgap energy with various thicknesses of Si NL along with (111) direction in the simulation result.

optimum process, as exhibited in Fig. 5(c). The result of simulated calculation demonstrates that the QC effect plays the main role as the nanolayer thickness is larger, in which the indirect bandgap is almost kept in thickness changing. In the same manner, the abrupt change effect in bandgap energy was discovered in the simulated calculation, where the bandgap energy deeply decreases as the nanolayer thickness arrives near the monoatomic layer, as shown in Fig. 5(d). Here, it should be noted that the bandgap rapidly disappears in the process.

The abrupt change effect in bandgap energy may be originated from transforming between different dimensions at the symmetry broken point. In picture (c) of Fig. 3, 4 or 5, the structure near the monoatomic layer belongs to the fractional dimension of 2.1–2.5 in the quasi-2D situation, and the bandgap will disappear to become a semi-metal, where new quantum phenomena and effects will appear in the process from the 3D layer to the quasi-2D shape and to the ideal quantum surface.

4. Conclusion

In summary, we have prepared the nanolayer structures with different thicknesses on silicon in the experiment, in which the new method of coherent electron beam irradiation and the PLD method were used. In the simulated calculation, the change ruler of bandgap energy with nanolayer thickness has been explored, where the abrupt change effect in bandgap energy was discovered as the nanolayer thickness decreases to arrive near the monoatomic layer, in which the Dirac-cone shape gradually occurs and the bandgap disappears in K space on quasi-2D silicene. The new effects will be explored deeply in the process from the 3D layer to the 2D structure of silicon. In the experiment, the thickness change can be controlled by manipulating

irradiation time and density of the coherent electron beam, which will provide an investigation platform on a quantum system of silicon.The results of simulating calculation demonstrated that the transformation from the indirect bandgap to the direct bandgap can be obtained really in the nanolayer of silicon growing along with (100) direction as the thickness is smaller than 10 nm, which has a good application on optic-electronic material and devices.

5. Methods

5.1. *Preparation of silicon nanolayers*

Preparation of silicon nanolayers involves two steps: fabrication of Si amorphous nanolayer by using PLD process and growth of Si nanolayer by using electron beam irradiation. In the first phase, a silicon wafer (100), (110) or (111) oriented substrate was taken on the sample stage in the combination fabrication system with pulsed laser etching (PLE) and pulsed laser deposition (PLD) devices. A pulsed Nd:YAG laser (wavelength: 1064 nm, pulse length: 60 ns FWHM, repetition rate: 1200) was used to etch lines on Si substrate in the PLE process. Then, the third harmonic of pulsed Nd:YAG laser at 355 nm was used to deposit the silicon amorphous nanolayer in the PLD process. In the second phase, we accelerate the electron beam from the field-emission electron gun by 200 KV and make it have higher energy and better coherence. The coherent electron beam with $0.5\,\mathrm{nA/nm^2}$ was used to irradiate on amorphous Si nanolayer for 10–30 min in Tecnai G2 F20 system, where the silicon nanolayers with various thicknesses rapidly grow, while the TEM images of nanolayers were taken at the same time. The thickness change of the Si NL can be controlled by modifying the irradiation time and density of the coherent electron beam.

5.2. *Transmission electron microscope analysis*

In the TEM (FEITecnai G2 F20) image, the various nanolayer structures of silicon are detected in vacuum (10^{-8}Pa), in which the electron beam from the field-emission electron gun is accelerated by 200 KV, and the compositions are measured on the samples by using analysis in X-ray energy spectra.

Acknowledgements

This work was supported by the National Natural Science Foundation of China (Grant Nos. 11847084). This work was supported by the Science Foundation of Guizhou (No. [2020]1Y022) and the Science Foundation of Guizhou University (Nos. 2017(03), 20185781-17).

References

1. S. Godefroo *et al.*, *Nat. Nanotech.* **3**, 174 (2008).
2. N. Daldosso *et al.*, *Phys.Rev. B* **68**, 085327 (2003).
3. M. Wolkin, J. Jorne, P. Fauchet, G. Allan and C. Delerue, *Phys. Rev. Lett.* **82**, 197 (1999).
4. L. Pavesi and R. Turan (eds.), *Silicon Nanocrystals; Fundamentals, Synthesis, and Applications* (Wiley-VCH, 2010).
5. N. Koshida (ed.), *Nanostructure Science and Technology: Device Applications of Silicon Nanocrystals and Nanostructures* (Springer, 2008).
6. F. Qian, S. Gradečak, Y. Li, C. Y. Wen and C. M. Lieber, *Nano Lett.* **5**, 2287 (2018).
7. B. Mayer, D. Rudolph, J. Schnell, S. Morkotter, J. Winner, J. Treu, K. Mculler, G. Bracher, G. Abstreiter, G. Koblmculler and J. J. Finley, *Nat. Commun.* **4**, 2931 (2013).
8. D. Saxena, S. Mokkapati, P. Parkinson, N. Jiang, Q. Gao, H. H. Tan and C. Jagadish, *Nat. Photonics* **7**, 963 (2013).
9. T. Bryllert, L. E. Wernersson, L. E. Froberg and L. Samuelson, *IEEE ElectronDevice Lett.* **27**, 323 (2006).
10. K. Tomioka, M. Yoshimura and T. Fukui, *Nature* **488**, 189 (2012).
11. J. Wallentin *et al.*, *Science* **339**, 1057 (2013).
12. B. Feng *et al.*, *Nano Lett.* **12**, 3507 (2012).
13. B. Lalmi *et al.*, *Appl. Phys. Lett.* **97**, 223109 (2010).
14. K. Takeda and K. Shiraishi, *Phys. Rev. B* **50**, 14916 (1994).
15. G. G. Guzmán-Verri and L. C. Lew Yan Voon, *Phys. Rev. B* **76**, 075131 (2007).
16. W. F. Tsai *et al.*, *Nat. Commun.* **4**, 1500 (2012).
17. T. Morishita, K. Nishio and M. Mikami, *Phys. Rev. B* **77**, 081401(R) (2008).
18. K. Nishio, T. Morishita, W. Shinoda and M. Mikami, *J. Chem. Phys.* **125**, 074712 (2006).
19. Y. Kanzawa *et al.*, *SolidState Commun.* **7**, 533–537 (1997).
20. F. Iacona, C. Bongiorno, C. Spinella, S. Boninelli and F. Priolo, *J. Appl. Phys.* **95**, 3723 (2004).
21. M. Zacharias *et al.*, *Appl. Phys. Lett.* **80**, 661 (2002).
22. C. Y. Liu, Z. C. Holman and U. R. L. Kortshagen, *Adv. Funct. Mater.* **20**, 2157 (2010).

23. L. Mangolini, E. Thimsen and U. Kortshagen, *Nano Lett.* **5**, 655 (2005).
24. D. Jurbergs, E. Rogojina, L. Mangolini and U. Kortshagen, *Appl. Phys. Lett.* **88**, 233116 (2006).
25. A. Gupta, M. T. Swihart and H. Wiggers, *Adv. Funct. Mater.* **19**, 696 (2009).
26. S. Niesar *et al.*, *Adv. Funct. Mater* **22**, 1190 (2012).
27. D. Alima, Y. Estrin, D. H. Rich and I. Bar, *J. Appl. Phys.* **112**, 114312 (2012).
28. C. H. Crouch *et al.*, *Appl. Phys. Lett.* **84**, 1850 (2004).
29. W. Q. Huang *et al.*, *Sci. Rep.* **4**, 9932 (2015).